Electronic Supplementary Information

A Layered Ultra-Stable Metal-Organic Framework for High-Loading of Zinc Single-Atom Oxygen Electrocatalyst

Sanjit Kumar Parida,* Arindam Das

Surface & Sensors Studies Division, Materials Science Group, Indira Gandhi Centre for Atomic Research, A CI of Homi Bhabha National Institute, Kalpakkam 603102, Tamilnadu, India

1. Experimental Section

1.1 Synthesis

Synthesis of ZIF-7-III was carried out at room temperature by mixing weighted quantity of $Zn(NO_3)_2.6H_2O$ and benzimidazole dissolved in 100 ml methanol each. The metal:linker ratio was maintained at 1:4 by mole. The mixture solution was stirred for 30 mins and then allowed to rest for 12 hours followed by centrifugation, washing with methanol and drying under vacuum at 80˚C for overnight. As a control sample to highlight linker engineering approach, ZIF-8 was synthesized under similar condition except benzimidazole replaced by 2-methyl imidazole. The dried product was pyrolised at 800 / 900 / 1000 ˚C for 2 hrs at 5 ˚C/min heating rate under nitrogen flow to obtain the catalyst samples.

1.2 Chemical Stability Test

Weighed amount of ZIF-7-III (≈ 200 mg) was dispersed in 500 ml of methanol, water, benzene and 0.1M KOH maintained at 65 °C, 100 °C, 80 °C and 100 °C respectively and kept for 5 days with stirring. After 5 days the MOF samples were washed repeatedly using DI water, dried under vacuum for further characterization.

1.3 Characterization

The morphology and structure of the samples were characterized by field-emission scanning electron microscopy (FESEM; Cross-Beam 340, Carl Zeiss) and transmission electron microscopy (Thermo Fisher Scientific, Talos F200S, G2). High-angle annular dark-field scanning transmission electron microscopy (HAADF-STEM) images were acquired with a JEOL JEM ARM 300 F2 probe-corrected transmission electron microscope with aberration correction. X-ray absorption fine structure (XAFS) spectroscopy experiments including the X-ray absorption near edge structure (XANES) and extended X-ray absorption fine structure (EXAFS), were carried out at the BL-9 beamline of the Raja Raman Centre for Advanced Technology, India. All samples were characterized using Zn-K edge XANES and EXAFS in transmission mode under ambient conditions, using Zn foil as a reference. A Si (111) double crystal was used for energy selection. The data reduction, analysis and EXFAS fitting were performed with Athena, Artemis and IFEFFIT software package. The surface properties of the samples were analysed by X-ray photoelectron spectrometer (K-Alpha, Thermo Scientific) using Al Kα as X-ray source. The Binding Energy (BE) was calibrated using C1s peak and CasaXPS was used for data analysis. The Zn content of the samples were determined by ICP-OES (AMETEK, Spectro Arcos, Germany). Powder X-ray diffraction (XRD) patterns were recorded using a Bruker D8 Advance diffractometer with Cu Kα radiation (λ = 1.5406 Å, 35 kV). Bruker Vertex 70 Fourier Transform Infrared (FT-IR) spectrometer in the range of 4000–400 cm^{-1} at a spectral resolution of 0.5 cm^{-1}. Raman spectra were collected using a confocal Raman spectroscope (alpha300 RA, WITec, 532 nm). The N_2 sorption isotherms are collected using a Quantachrome instruments Autosorb iQ station at liquid-nitrogen temperature.

Electrochemical measurements

The electrochemical performance was performed on a WaveDriver 200 (Pine Research Instrumentation) electrochemical workstation with a three-electrode system having a carbon rod as the counter electrode, Hg/HgO (CHI152) electrode as the reference electrode and a glassy carbon (GC) disk with platinum ring electrode (RRDE, disk diameter = 5.61 mm) as the substrate for the working electrode. The catalyst ink was coated on the glassy carbon and used as the working electrode. In a typical procedure, 5 mg of the catalysts were dispersed in 200 µl DI water, 290 µl isopropanol and 10 µl 5% Nafion mixed solution to form a homogeneous catalyst ink under ultrasonic conditions for 40 min. A certain volume of the ink was

dropped on the GC surface and dried at a room temperature to give a 800 μg cm^{-2} loading for all samples excluding commercial Pt/C (20 wt%, Fuel Cell Store, USA) which was loaded at 20 $\mu g_{Pt}\, cm^{-2}$. All the tests were carried out in 0.1M KOH solution. All collected potential data were transformed to standard reversible hydrogen electrode (RHE) following the equation:

$E_{(RHE)} = E_{(Hg/HgO)} + 0.874 - iR$

The solution resistance is determined by the high-frequency intercept from the Nyquist plot obtained by the electrochemical impedance spectroscopy (EIS) technique. The cyclic voltammetry results were conducted in Ar- and O_2-saturated 0.1M KOH with a scan rate of 10 mV s^{-1}. RDE tests were conducted by linear sweep voltammetry (LSV) in O_2-saturated 0.1M KOH at different rotation rates with a sweep rate of 10 mV s^{-1}. The stability tests (accelerated stress tests) were carried out at room temperature in O_2-saturated 0.1M KOH solution by continuous potential cycling between 0.6 and 1.0 V vs RHE at a scan rate of 50 mV s^{-1} for 5,000 cycles. The chronoamperometry (CA) tests were performed at room temperature in O_2-saturated 0.1M KOH solution by applying a potential of 0.8 V for 25 hrs.

The kinetic current density (J_K) and the electron transfer number (n) was calculated from the Koutecky-Levich (K-L) equation (1) from the plot of 1/J vs $1/\omega^{1/2}$.

$$\frac{1}{J} = \frac{1}{J_L} + \frac{1}{J_K} = \frac{1}{B\omega^{1/2}} + \frac{1}{J_K}$$

$$B = 0.62nFC_O D_O^{2/3} \nu^{-1/6} \quad (1)$$

where J, J_K, and J_L are the measured, kinetic and diffusion-limiting current densities respectively, ω is the angular velocity (rad s^{-1}), n is the number of transferred electrons per oxygen molecule, F is the Faraday constant (96485 C mol^{-1}), C_O is the bulk concentration of O_2 (1.2×10^{-6} mol·cm^{-3}), D_O is the diffusion coefficient of O_2 in 0.1M KOH (1.9×10^{-5}·cm^2·s^{-1}) and ν is the kinematic viscosity of the electrolyte (0.01 $cm^2.s^{-1}$).

The percentage of peroxide yield (H_2O_2%) and the electron transfer number (n) was determined by the following equations (2) from RRDE test.

$$H_2O_2(\%) = 200 \times \frac{\frac{I_R}{N}}{I_D + \frac{I_R}{N}}$$

$$n = 4 \times \frac{I_D}{I_D + \frac{I_R}{N}} \quad (2)$$

Where, I_D is the disk current, I_R is the ring current, and N is the ring current collection efficiency (0.37) of the Pt ring.

Electrochemical surface area (ECSA) was calculated from the electrochemical double layer capacitance as follow:

$$ECSA = \frac{C_{dl}}{C_s} \times S \quad (3)$$

Where, Cdl = double layer capacitance determined from cyclic voltammetry, Cs = capacitance, S = geometric area of electrode. An average value of Cs =22 μF cm^{-2} was used in this work for ECSA calculation with Cs being the capacitance of an atomically smooth planar surface of the material per unit area under identical electrolyte conditions.[1, 2]

The mass actvity (J_M) of the catalysts at 0.8 V were determinsed by using equation (4):

$$J_M = \frac{J}{C_M} \quad (4)$$

Where, J = current density at 0.8 V and C_M = metal loading on the electrode (mgcm^{-2}).

The turn-over frequency (TOF) at 0.8 V was estimated by equation (5):

$$TOF = \frac{J_K \times N_e}{w_M \times C_m \times N_A/M_A} \quad (5)$$

Where, J_K = kinetic current density at 0.8 V (Acm^{-2}), N_e = electron number per Coulomb (6.24×10^{18}), w_M = metal content in the catalyst (%), C_m = catalyst loading on the electrode (gcm^{-2}), N_A = Avogadro constant (6.022×10^{23}) and M_A = molar atomic mass of the element ($gmol^{-1}$).

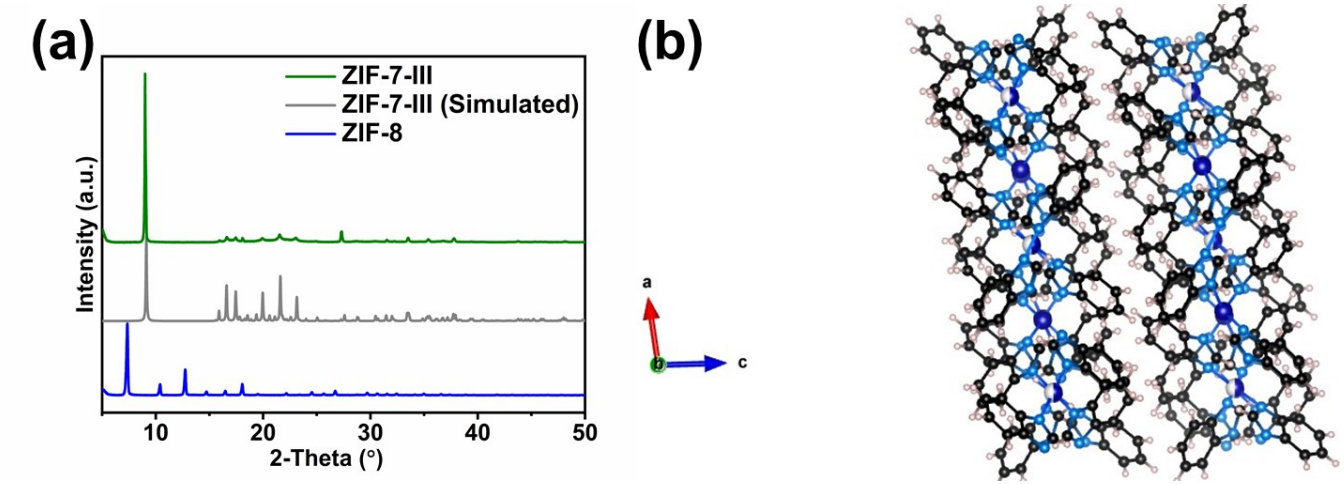

Fig. S1 (a) Powder XRD patterns of ZIF-8 and ZIF-7-III (b) Layered structure of ZIF-7-III generated using CIF file in Vesta.

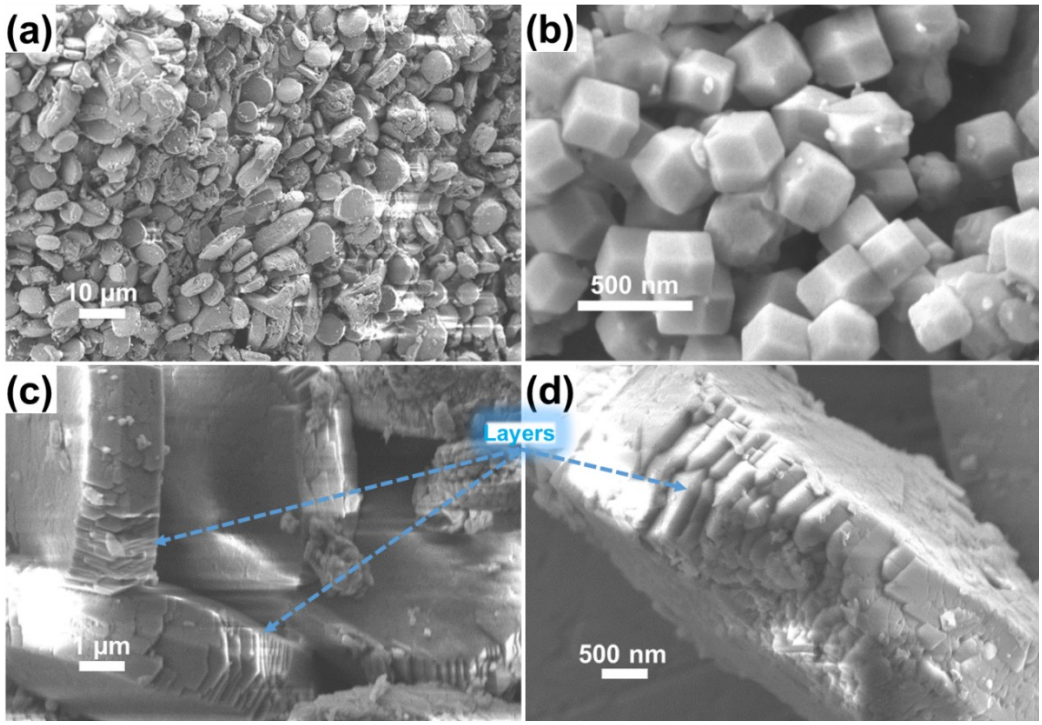

Fig. S2 Representative FESEM images of (a) ZIF-7-III (b) ZIF-8 and (c)-(d) ZIF-7-III showing layered structure.

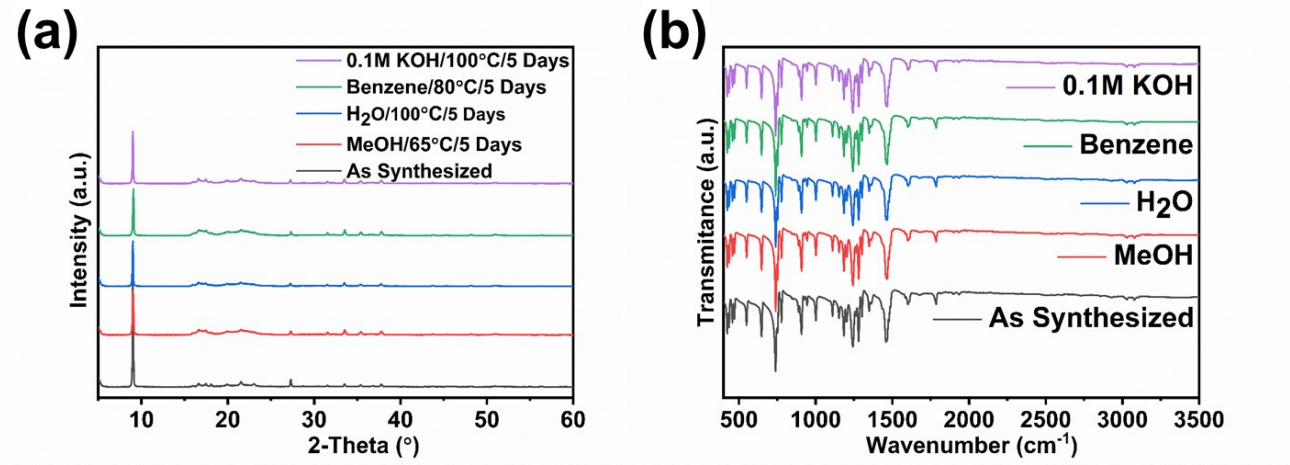

Fig. S3 (a) Powder XRD patterns and (b) FTIR spectrum of ZIF-7-III showing chemical stability of the MOF.

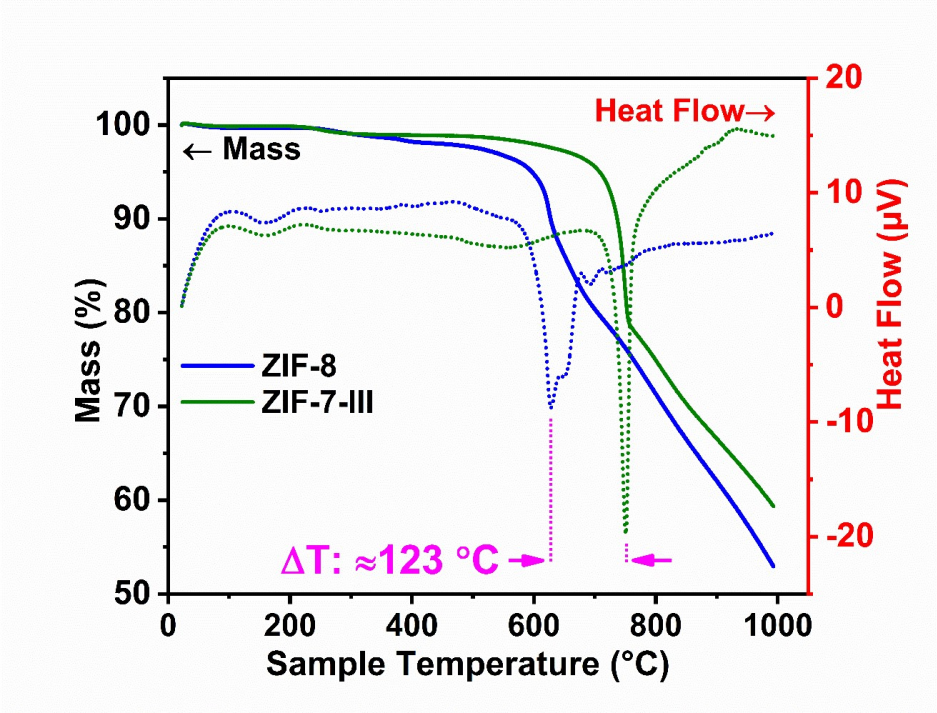

Fig. S4 TGA curves of ZIF-8 and ZIF-7-III recorded in Ar atmosphere with 10˚C/min heating rate.

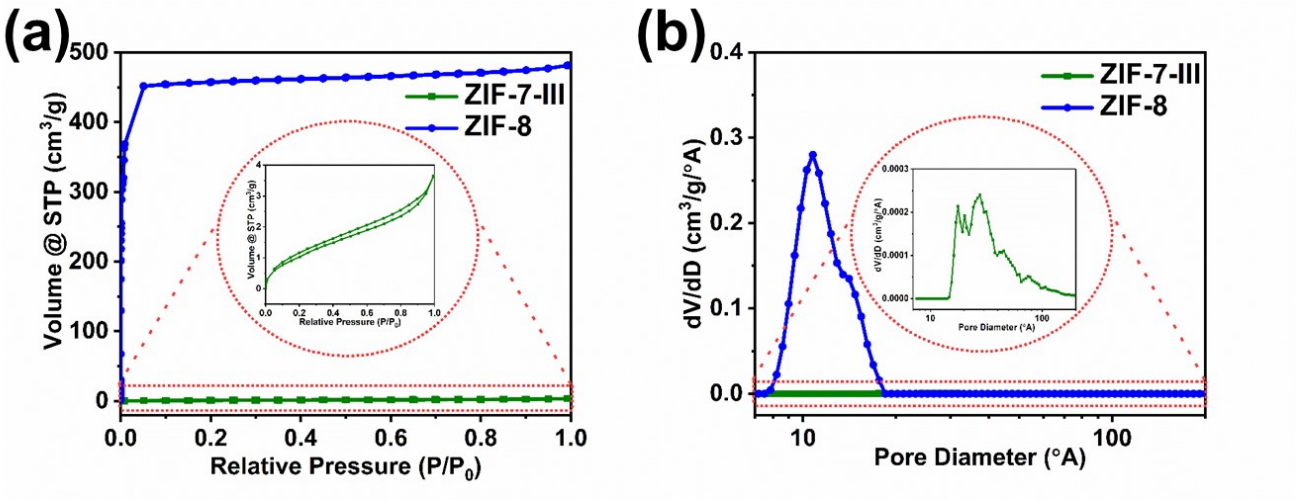

Fig. S5 (a) N_2 adsorption-desorption isotherms and (b) Pore size distribution of ZIF-7-III and ZIF-8.

Table S1. BET surface area and pore volume of the MOFs.

Catalyst	SA_{BET} (m^2/g)	SA_{Micro} (m^2/g)	V_{Micro} (cc/g)	V_{Meso} (cc/g)	V_{Total} (cc/g)
ZIF-8	1934.3	1888.8	0.688	22.0	0.042
ZIF-7-III	4.3	0.0	0.000	1.9	0.004

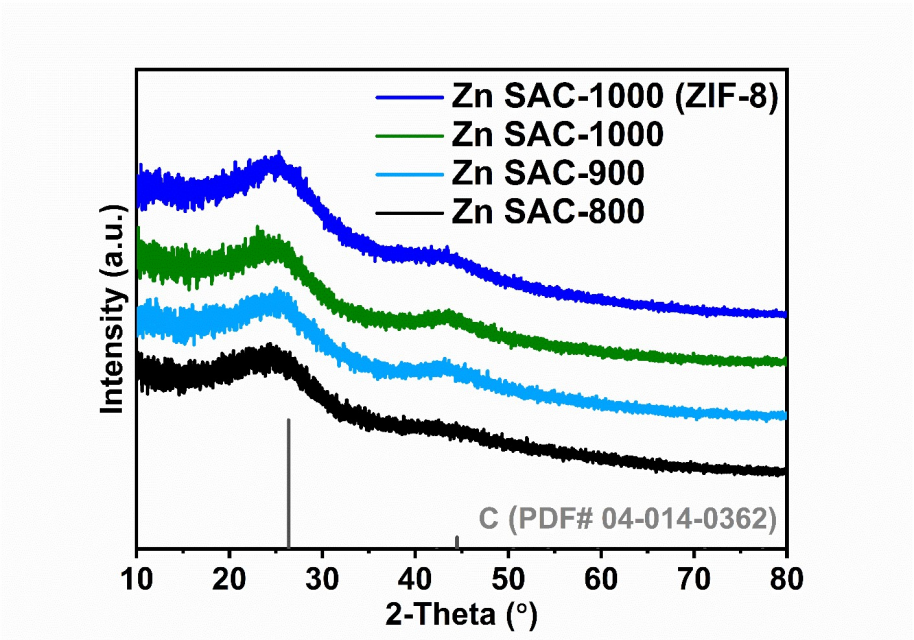

Fig. S6 Powder XRD patterns of the Zn-N-C catalysts derived from ZIF-8 and ZIF-7-III.

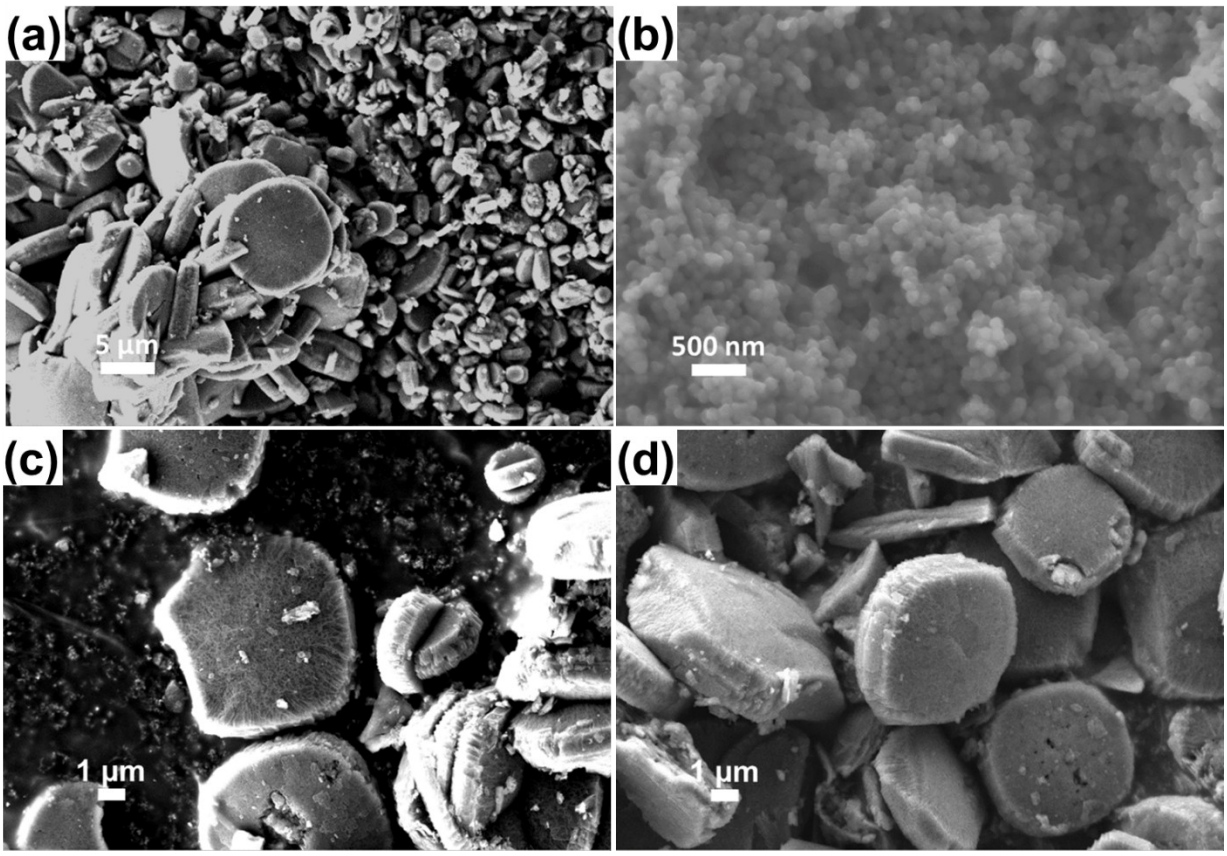

Fig. S7 Representative FESEM images of (a) Zn SAC-1000 (b) Zn SAC-1000 (ZIF-8) (c) Zn SAC-900 and (d) Zn SAC-800.

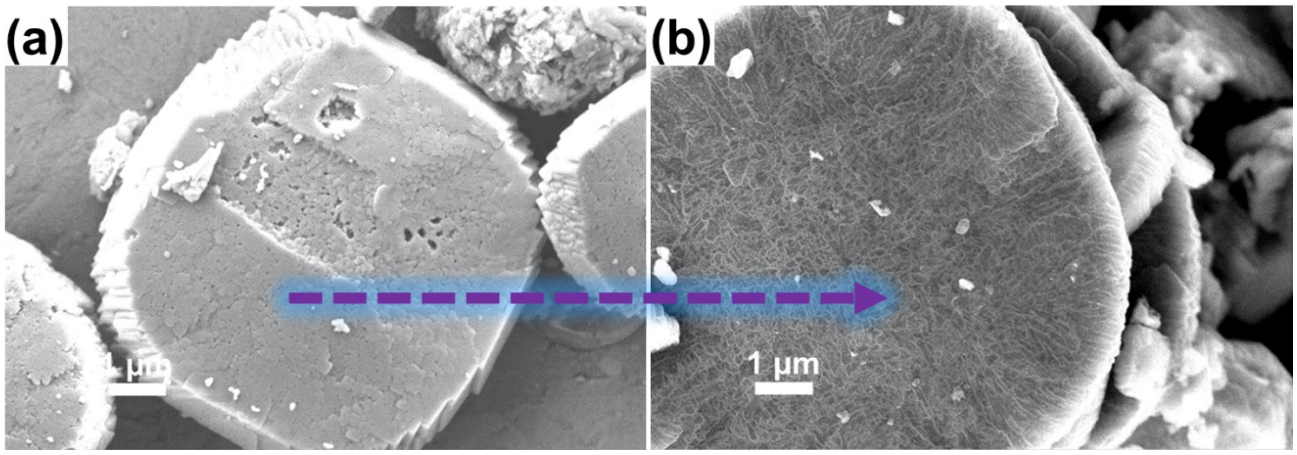

Fig. S8 Representative FESEM images of (a) ZIF-7-III and (b) Zn SAC-1000 showing surface transformation during pyrolysis.

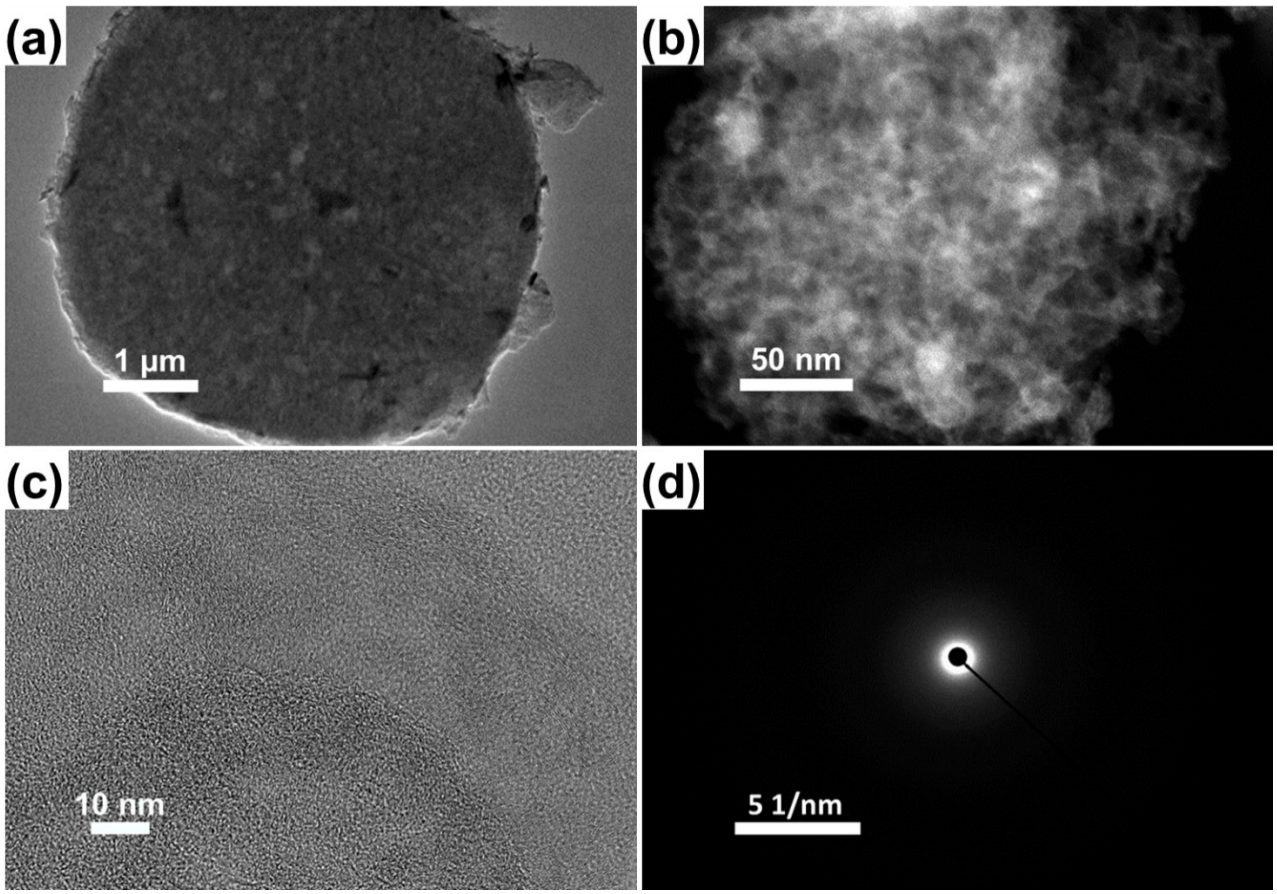

Fig. S9 Representative (a) TEM image (b) DF-STEM image (c) HRTEM image and (d) SAED pattern of Zn SAC-1000.

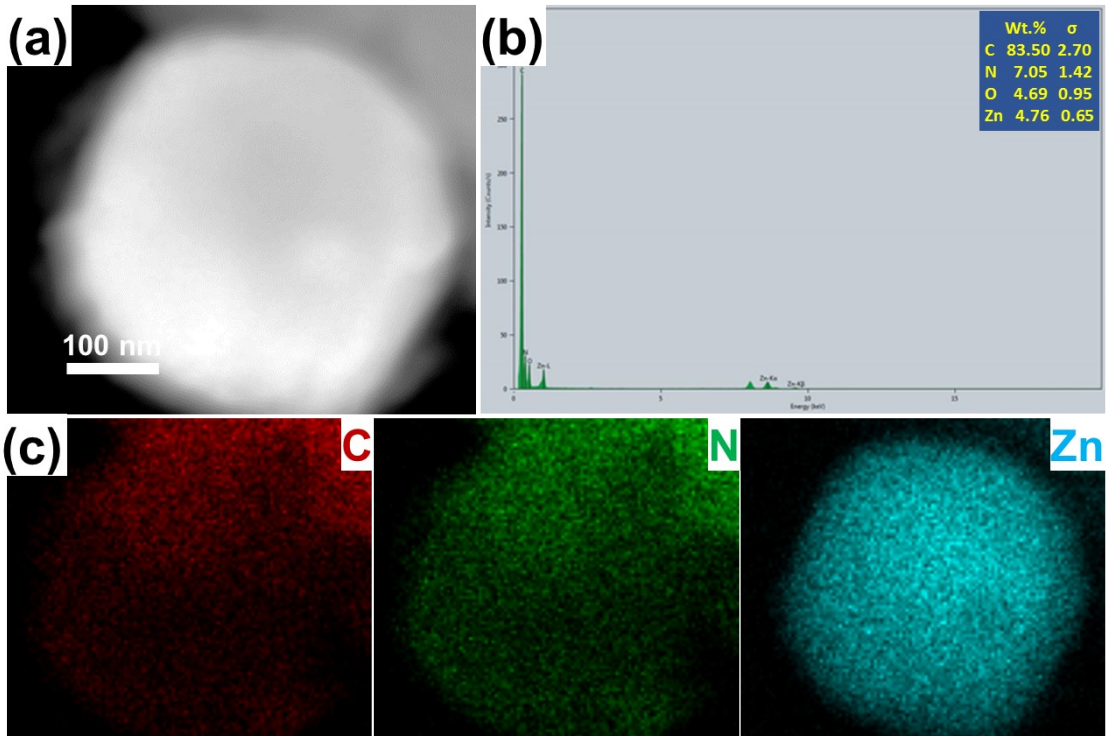

Fig. S10 Representative (a) STEM image (b) EDX spectrum and (c) Corresponding elemental mapping results of Zn SAC-1000 catalyst.

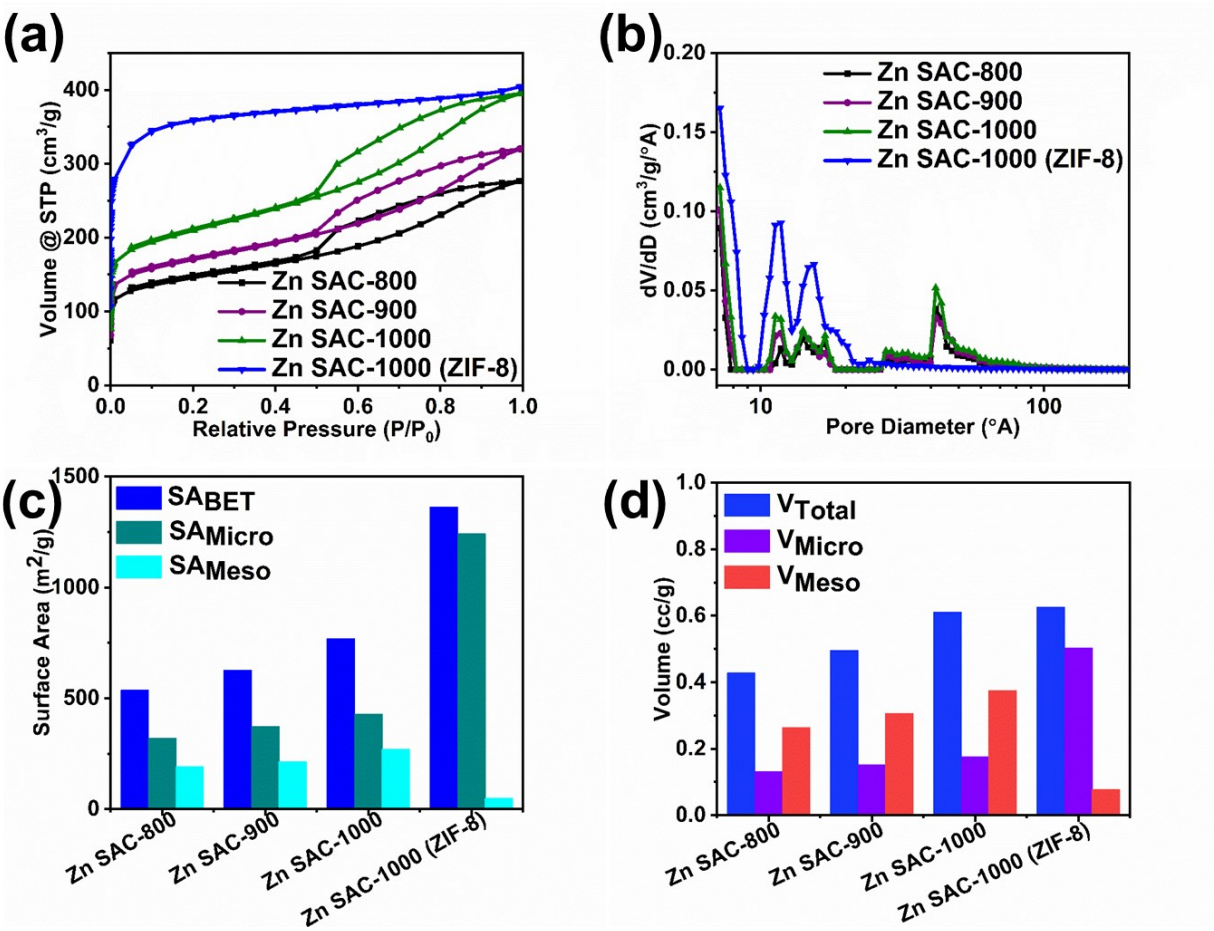

Fig. S11 (a) N_2 adsorption-desorption isotherms (b) Pore size distribution (c) Surface area and (d) Pore volume fraction of Zn SAC derived from ZIF-7-III and ZIF-8.

Table S2. BET surface area and pore volume of the catalysts.

Catalyst	SA_{BET} (m^2/g)	SA_{Micro} (m^2/g)	V_{Micro} (cc/g)	V_{Meso} (cc/g)	V_{Total} (cc/g)
Zn SAC-800	536.9	319.4	0.131	191.8	0.264
Zn SAC-900	627.4	373.0	0.152	214.3	0.306
Zn SAC-1000	769.0	428.6	0.176	271.1	0.375
Zn SAC-1000 (ZIF-8)	1362.8	1242.7	0.503	48.3	0.078

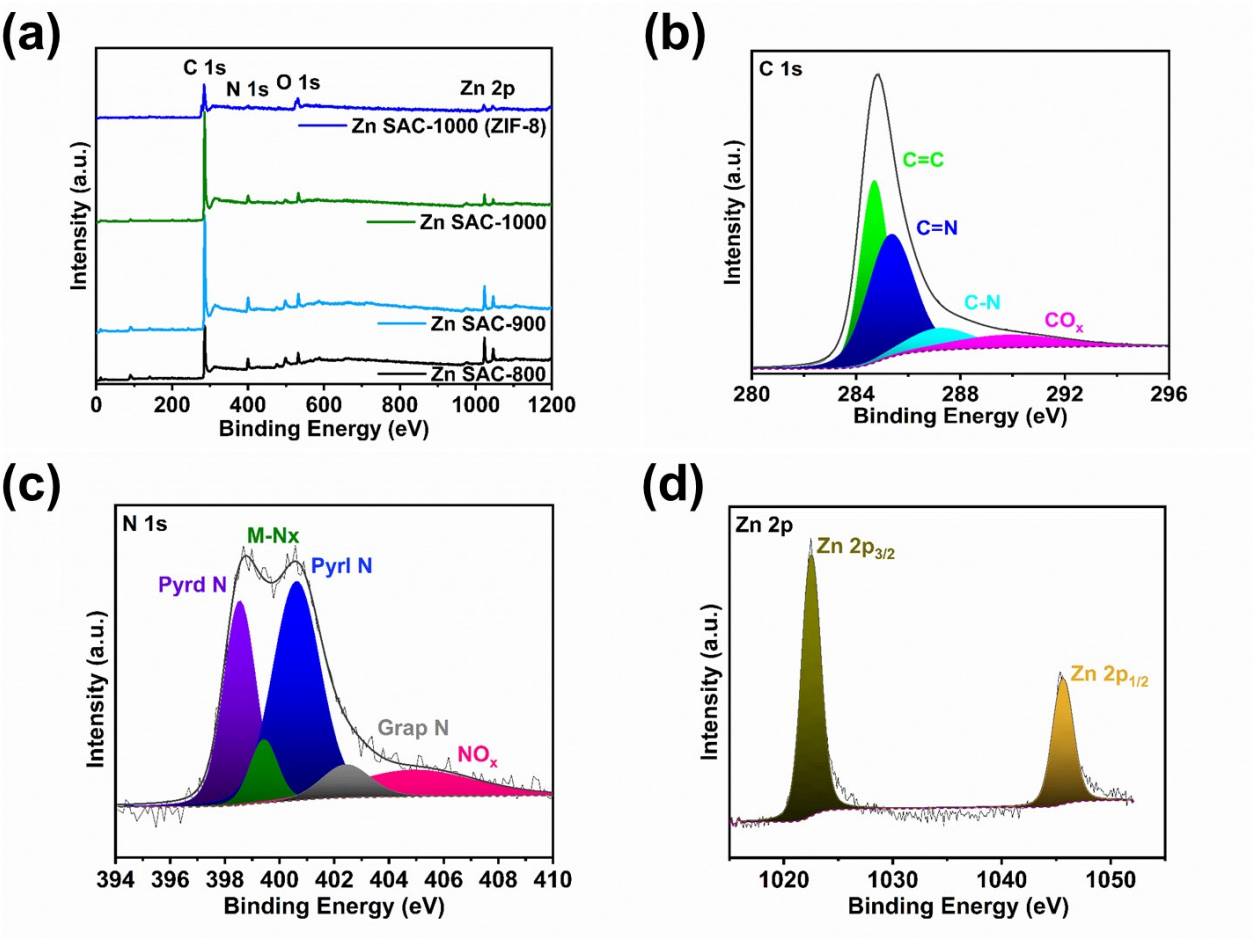

Fig. S12 (a) XPS survey spectra and high-resolution XPS spectra of (b) C 1s, (c) N 1s and (d) Zn 2p in Zn SAC derived from ZIF-7-III.

Table S3. Elemental composition of catalysts as obtained from XPS and ICP-OES.

Catalyst	XPS (at.%)				ICP-OES (wt.%)
	C	N	O	Zn	Zn
Zn SAC-800	78.48	11.72	6.48	3.32	11.55
Zn SAC-900	85.35	8.02	5.03	1.60	6.06
Zn SAC-1000	89.09	5.83	4.24	0.85	2.52
Zn SAC-1000 (ZIF-8)	82.59	4.80	11.92	0.69	2.10

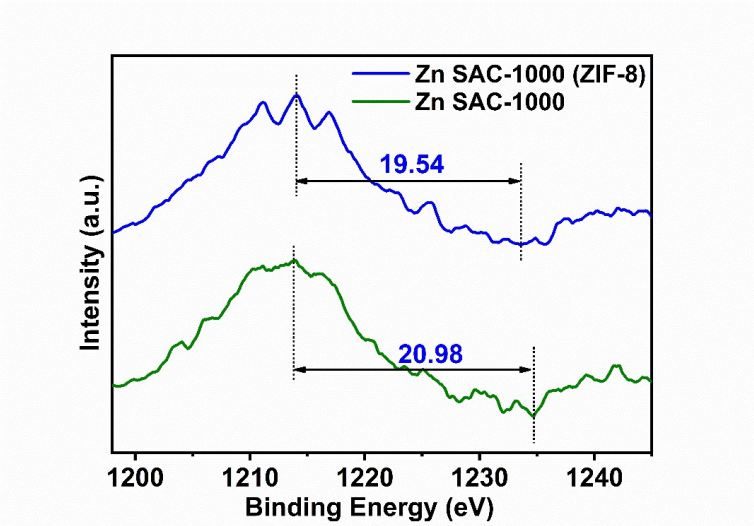

Fig. S13 C KLL Auger spectra of carbon in the catalyst samples.

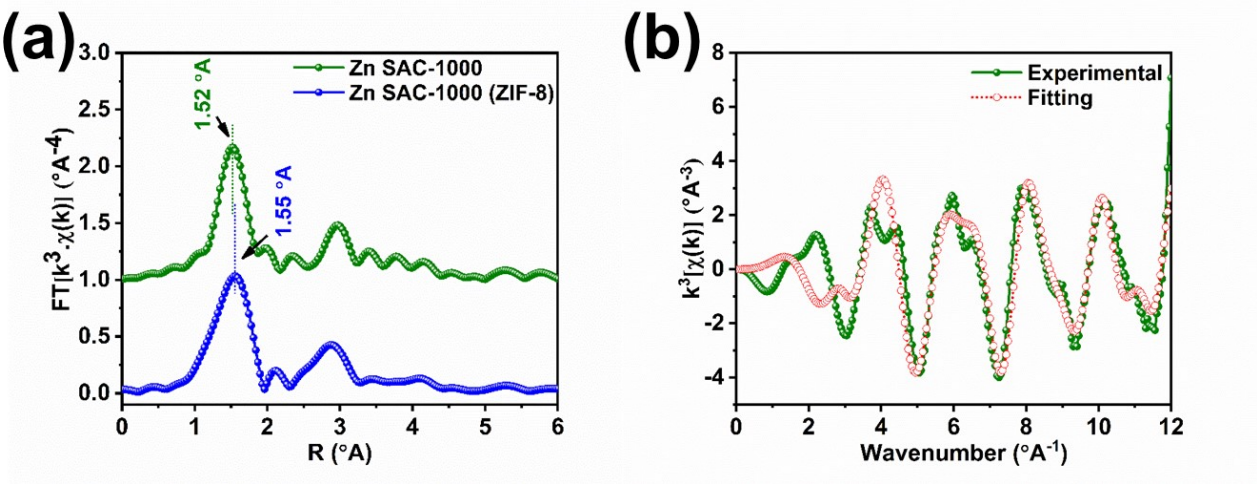

Fig. S14 (a) Comparison of the FT-EXAFS of Zn SAC-1000 and Zn SAC-1000 (ZIF-8) catalysts showing Zn-N bond lengths (b) The experimental and fitting curves of the EXAFS pattern of Zn SAC-1000 with the model structure in k-space.

Table S4. Fitting parameters of Zn K-edge EXAFS for Zn SAC-1000 catalyst.

Sample	CN	R (°A)	σ^2 ($\times10^{-3}$)	ΔE_0 (eV)	R-factor
Zn SAC-1000	4	1.97±0.03	3.7	-3.64	0.010

CN: coordination number; R: the distance between absorber and backscatter atoms (equals to the bond length of Zn-N); σ^2: the Debye-Waller factor value; ΔE_0: the inner potential correction to account for the difference in the inner potential between the sample and the reference compound.

Error bounds that characterize the structural parameters obtained by EXAFS spectroscopy were estimated as R ± 1%; σ^2 ± 20%; ΔE_0 ± 20%.

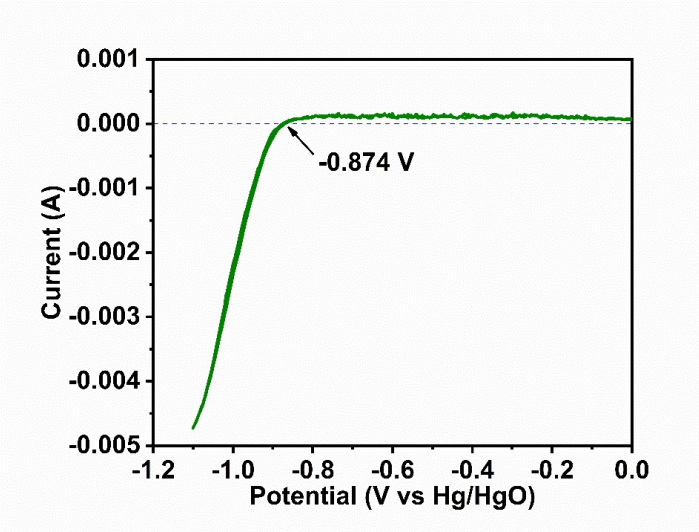

Fig. S15 Calibration graphs of Hg/HgO reference electrode.

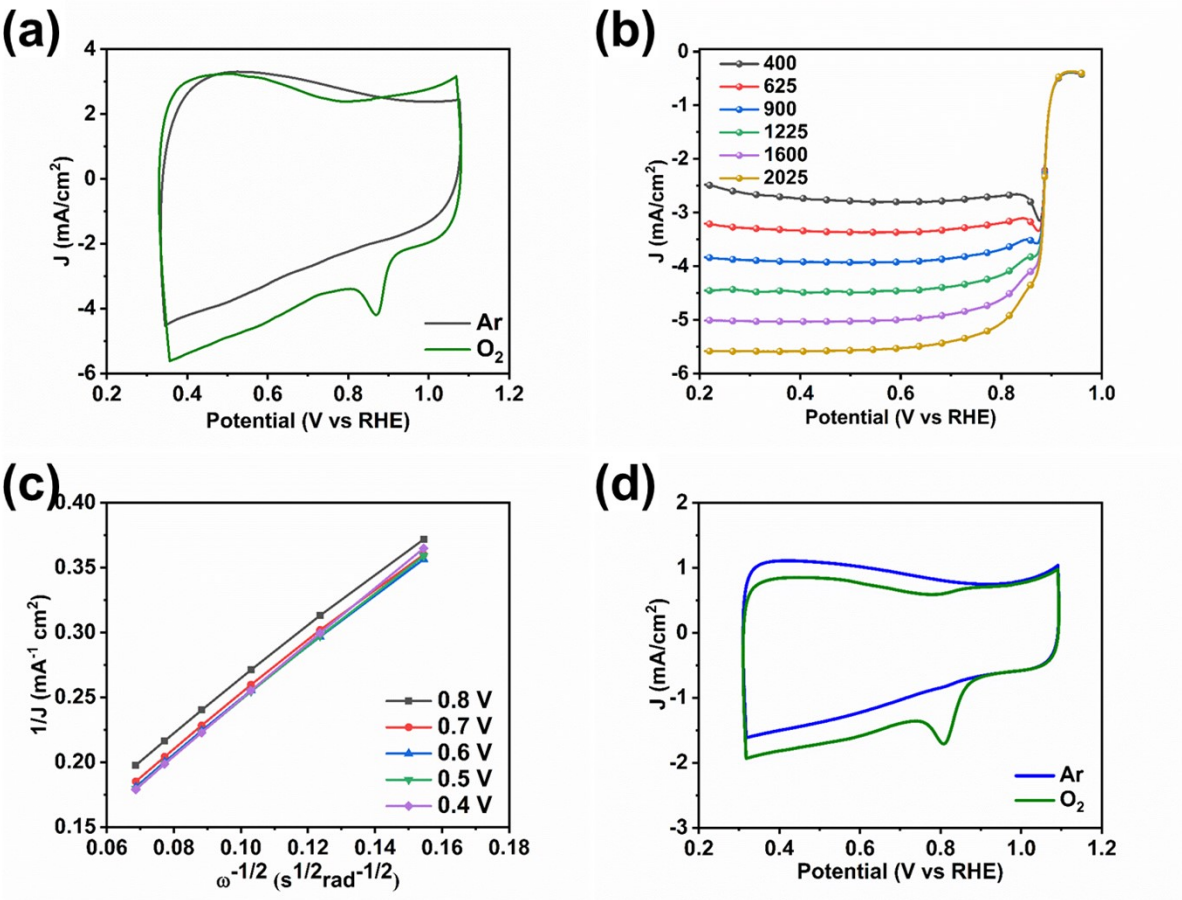

Fig. S16 Electrochemical performance of the catalysts showing (a) CV (b) LSV curves (c) K-L Plot of Zn SAC-1000 and (d) CV curves of Zn SAC-1000 (ZIF-8).

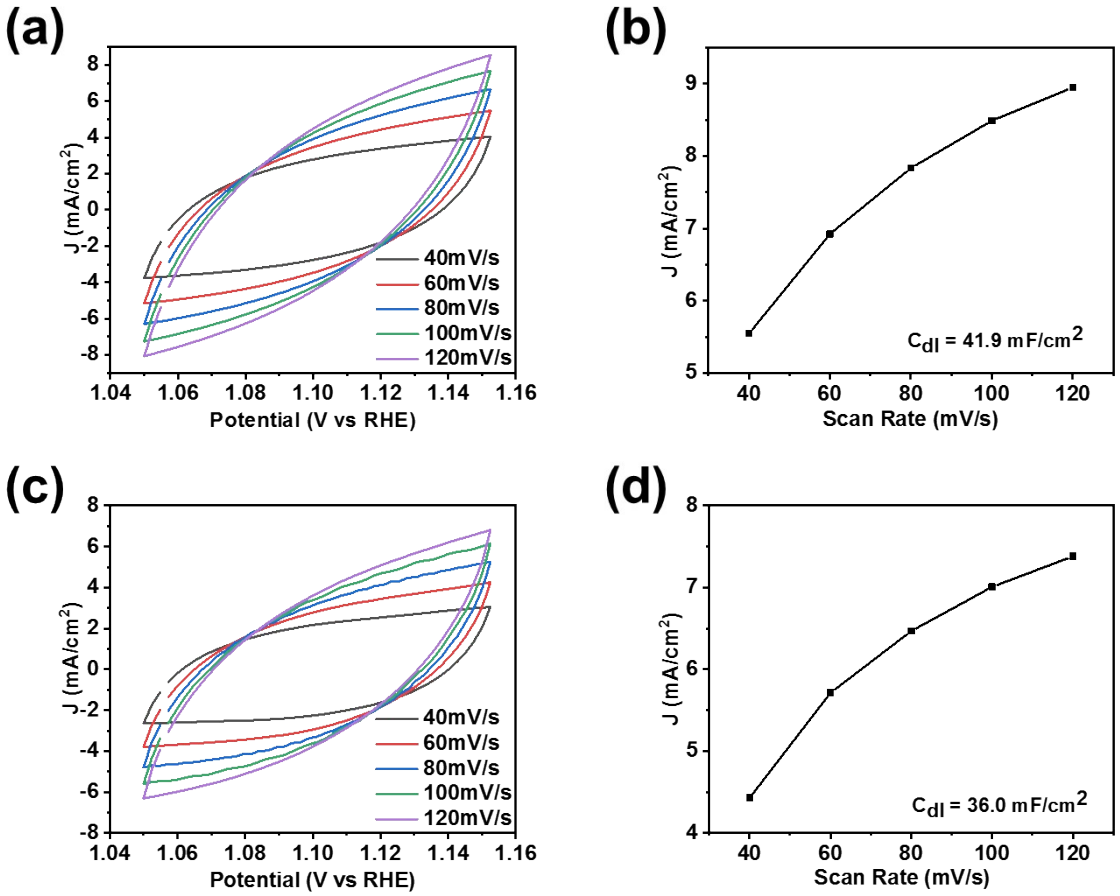

Fig. S17 Representative double-layer capacitance measurements showing (a)-(c) CV curves and (b)-(d) Capacitive current against the scan rates of Zn SAC-1000 and Zn SAC-1000 (ZIF-8) respectively.

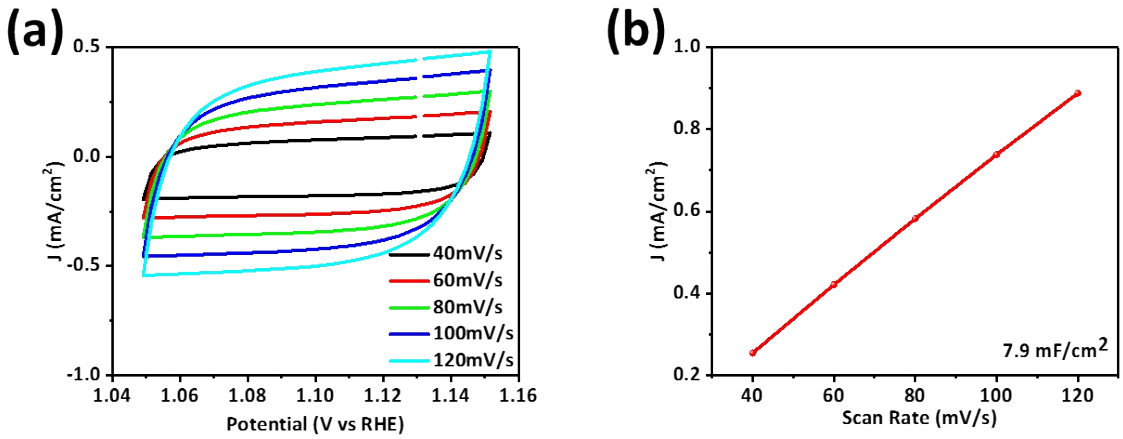

Fig. S18 Double-layer capacitance measurements showing (a) CV curves and (b) Capacitive current against scan rates of Pt/C.

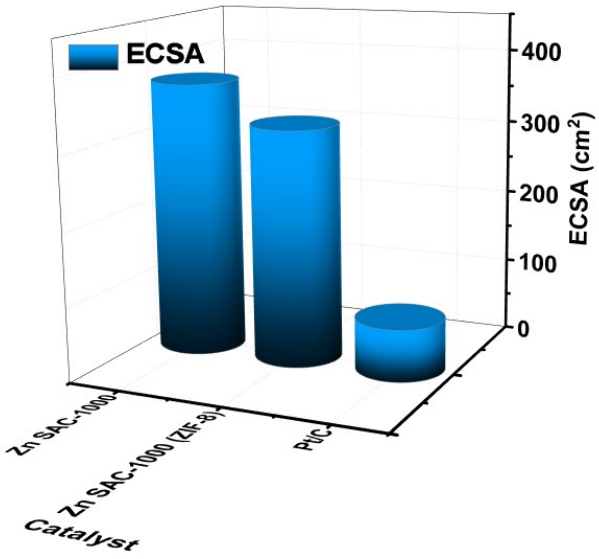

Fig. S19 ECSA of the catalysts.

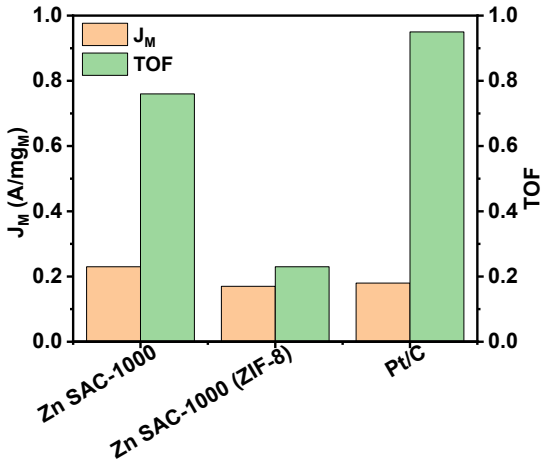

Fig. S20 S Mass activity and TOF of the catalysts at 0.8 V.

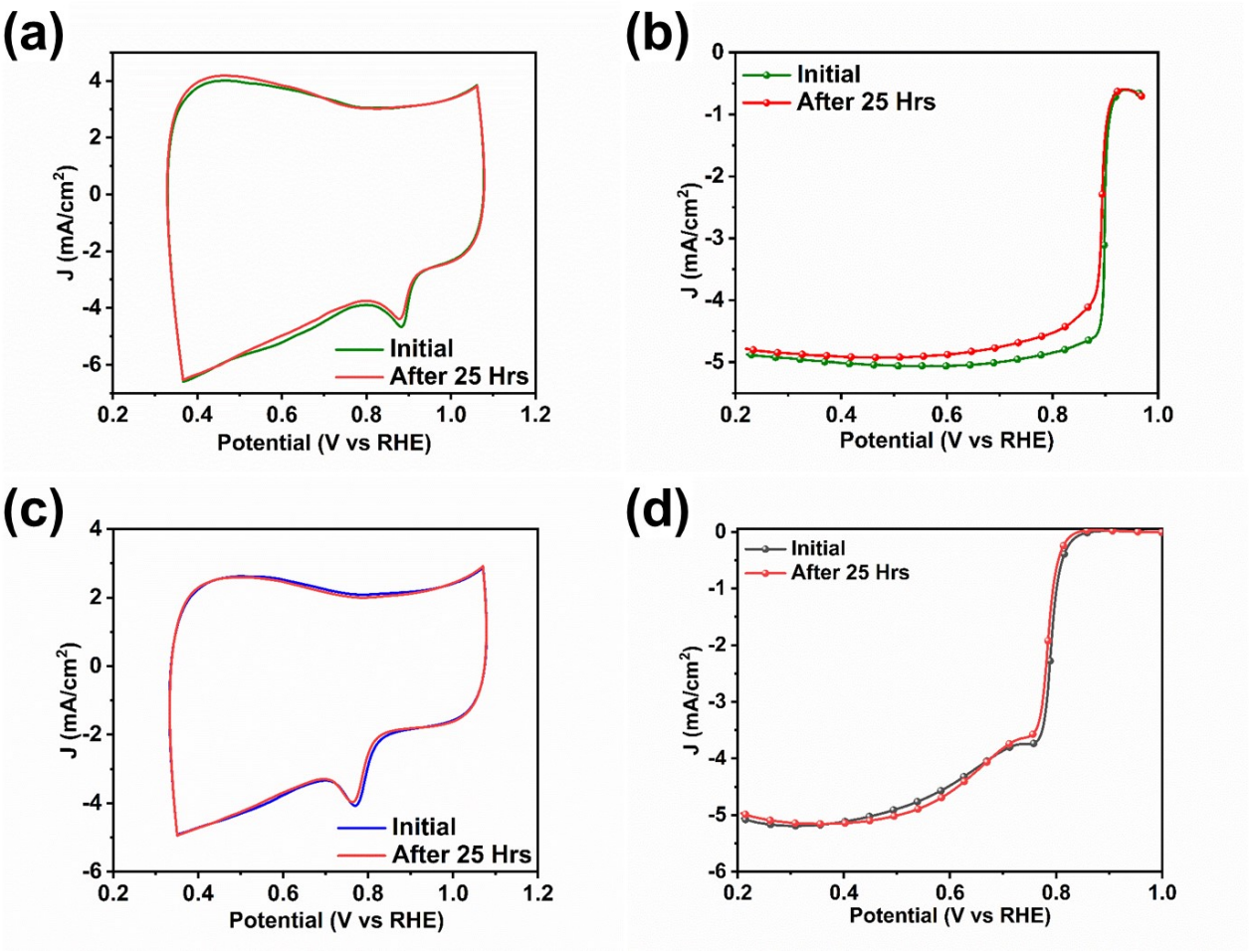

Fig. S21 (a) CV (b) LSV curves of Zn SAC-1000 and (c) CV (d) LSV curves of Zn SAC-1000 (ZIF-8) during chronoamperometric test at 0.8V vs RHE for 25 hrs at 1600 RPM in O_2 saturated 0.1M KOH.

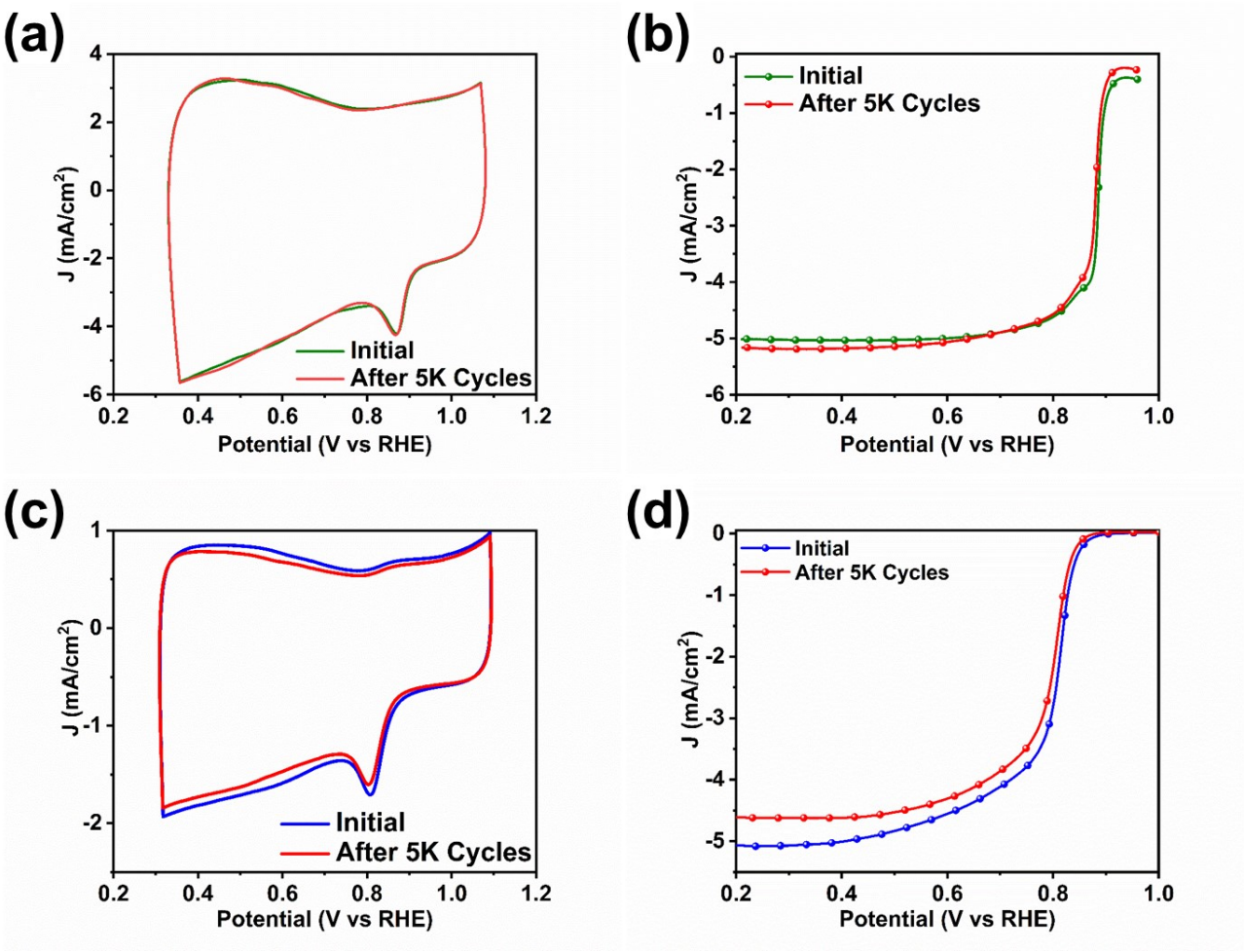

Fig. S22 (a) CV (b) LSV curves of Zn SAC-1000 and (c) CV (d) LSV curves of Zn SAC-1000 (ZIF-8) during AST.

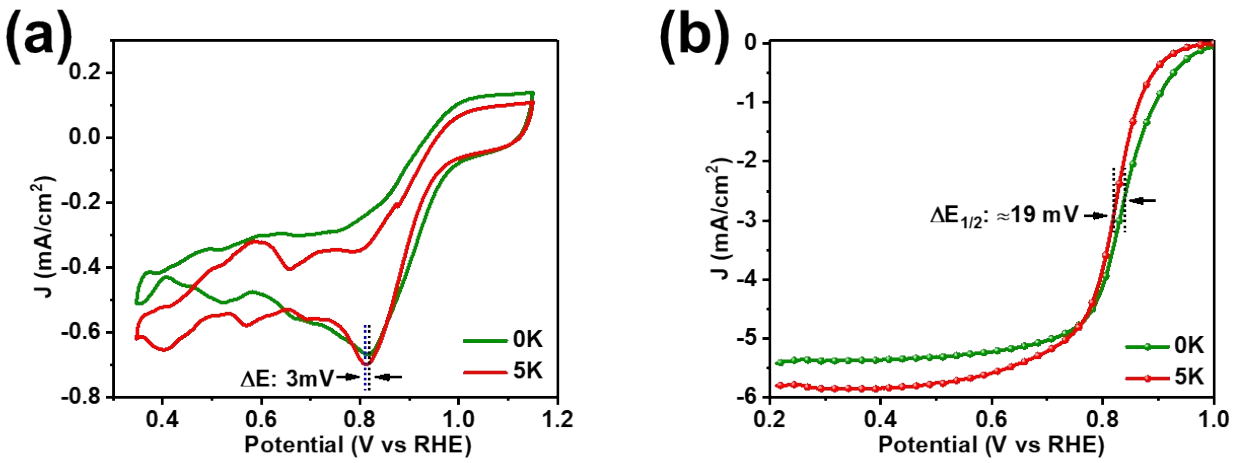

Fig. S23 (a) CV and (b) LSV curves of Pt/C after potential cycling experiment for 5000 cycles in 0.1M KOH.

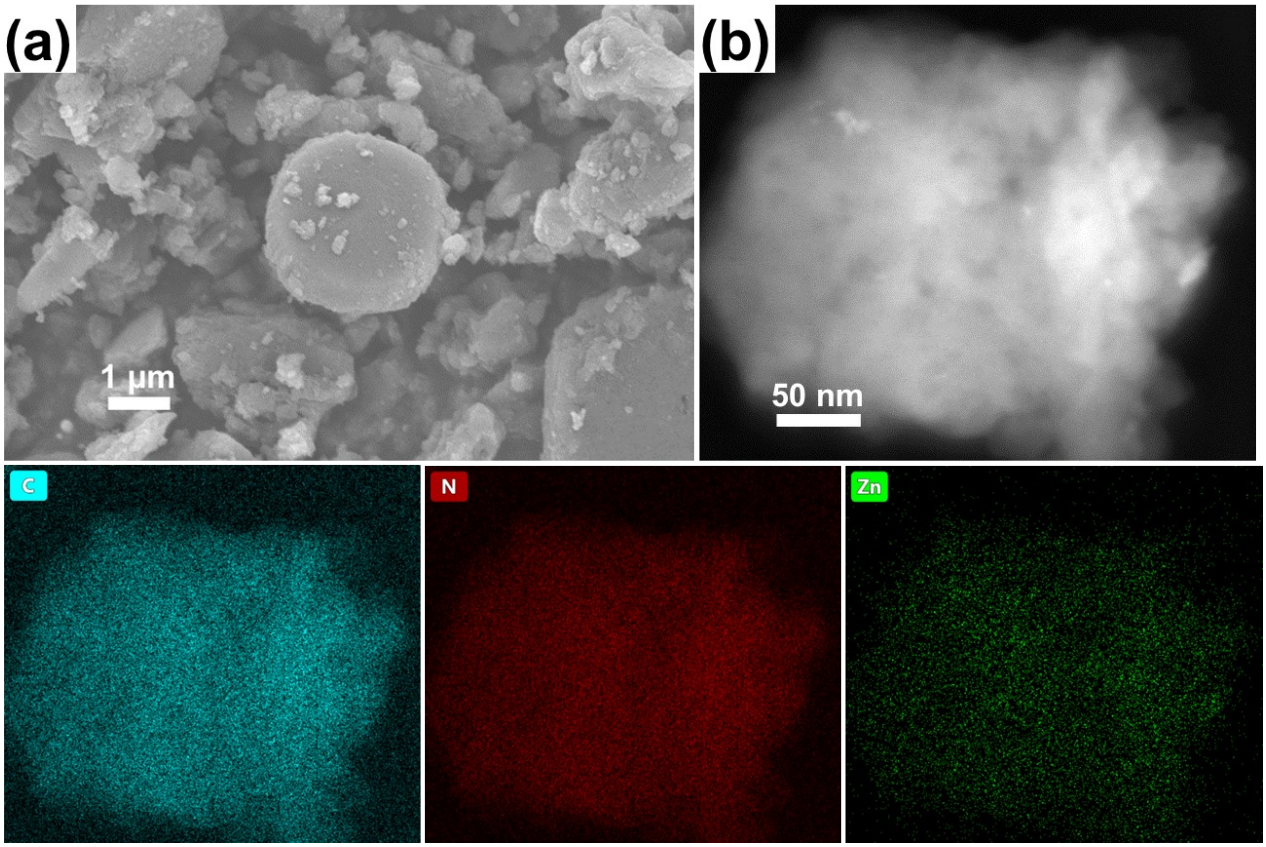

Fig. S24 Representative (a) FS-SEM image (b) STEM image with corresponding elemental mapping results of Zn SAC-1000 after AST.

Table S5. Review of ORR activity of Zn SACs in 0.1M KOH as reported in recent literature.

Catalyst	Zn Content	Loading ($\mu g/cm^2$)	$E_{1/2}$ (V vs RHE)	$\Delta E_{1/2}$ (mV during AST)	J_K (mA/cm^2)	Ref.
Zn SAC-1000	**2.52 wt%**	**800**	**0.886**	**6.1 (5k Cycles)**	**21.1 @ 0.7 V 16.6 @ 0.8 V**	**This work**
ZnNC-10	0.76 at%	255	0.875	-	-	[1] J. Power Sources 656 (2025) 238102
ZnNC-3	1.5 wt%	500	0.840	-	-	[2] J. Environ. Chem. Eng. 12 (2024) 113616
Zn/NC-2	6.10 wt%	200	0.845	-	7.63 @ 0.8 V	[3] Inorg. Chem. 2023, 62, 40, 16547–16553
Zn-N-C-2	0.95 wt%	620	0.850	10 (5k cycles)	-	[4] J. Colloid Interface Sci. 650 (2023) 934–942
ZnN_4P/C	6.23 wt%	200	0.860	5 (8k cycles)	-	[5] Chinese J. Catal. 43 (2022) 2193–2201
Zn–SAs/UNCNS	0.47 wt%	250	0.910	6 (5k cycles)	8.66 @ 0.9 V	[6] Chem. Catalysis 2 (2022) 836–852
Zn-N-C-1	5.64 wt%	500	0.873	0.54 (1k cycles)	-	[7] Angew. Chem. Int. Ed. 2019, 58,7035–7039
ZnN_X/BP	0.3 wt%	390	0.850	35 (20k cycles)	-	[8] Adv. Funct. Mater. 2017, 27, 1700802

References

1. A. Jaiswal, R. Kumar and R. Prakash, ACS Applied Energy Materials, 2023, 6, 7803-7817.
2. C. C. L. McCrory, S. Jung, J. C. Peters and T. F. Jaramillo, Journal of the American Chemical Society, 2013, 135, 16977-16987.